buildings

MDPI

Article

Development and Mechanical Property Analysis of a Novel Uplift Pile Incorporating Composite Anchors

Zongyuan Mao [1,2,3], Jiaqi Jiang [4], Hao Guo [3] and Enzhi Wang [1,*]

[1] State Key Laboratory of Hydroscience and Engineering, Tsinghua University, Beijing 100084, China; 13910109701@126.com
[2] China Academy of Building Research, Beijing 100013, China
[3] China Building Technique Group Co., Ltd., Beijing 100013, China; gh15935121011@163.com
[4] Key Laboratory of Urban Underground Engineering of Ministry of Education, Beijing Jiaotong University, Beijing 100044, China; 22125890@bjtu.edu.cn
* Correspondence: nzwang@tsinghua.edu.cn

Abstract: This paper presents a novel design for uplift piles incorporating a composite-anchor system. The composite-anchor system consists of steel strands, a non-expansion grouting body, and a high-strength steel pile. The aim of this design is to enhance the mechanical performance, durability, and economic efficiency of uplift piles. To evaluate the performance of the new pile, three sets of full-scale load tests were conducted, focusing on their in situ capacity, deformation, and stress characteristics. Despite a significantly lower reinforcement ratio of 0.75% compared to conventional piles with a ratio of 3.84%, the new uplift piles exhibit an exceptional uplift bearing performance. The utilization of the lateral friction resistance of the lower pile body is significantly improved, leading to enhanced load distribution and stress transfer mechanisms. Furthermore, a numerical model was developed and validated against the experimental results, demonstrating its reliability in simulating the bearing characteristics of the new uplift piles. The multi-interface design of the composite-anchor system ensures the efficient transmission of internal forces induced by external uplift loads, resulting in an improved stress state within the pile body. Moreover, the multi-layer structure of the composite main bar enhances the durability of the uplift piles. In comparison to conventional piles, the new uplift pile design offers substantial advantages, including an 80% reduction in reinforcement ratio, a 65% reduction in reinforcement cage welding, a cost reduction of approximately 30%, and a shortened construction time by around 20%. These findings highlight the potential of the new composite-anchor-pile design to revolutionize the field of uplift pile applications, offering improved efficiency and effectiveness.

Keywords: uplift pile; composite anchor; in situ test; uplift capacity; construction technology

check for updates

Citation: Mao, Z.; Jiang, J.; Guo, H.; Wang, E. Development and Mechanical Property Analysis of a Novel Uplift Pile Incorporating Composite Anchors. *Buildings* **2023**, *13*, 2029. https://doi.org/10.3390/buildings13082029

Academic Editor: Suraparb Keawsawasvong

Received: 23 June 2023
Revised: 31 July 2023
Accepted: 7 August 2023
Published: 9 August 2023

Copyright: © 2023 by the authors. Licensee MDPI, Basel, Switzerland. This article is an open access article distributed under the terms and conditions of the Creative Commons Attribution (CC BY) license (https://creativecommons.org/licenses/by/4.0/).

1. Introduction

During the rapid development of urban economies, cities are facing challenges such as resource shortages and traffic congestion, commonly referred to as "urban diseases". The development and utilization of urban underground spaces (e.g., subways and underground shopping malls) are considered effective measures to address these issues [1–4]. As layout forms diversify, underground structures are extending deeper. In specific cases (such as areas with high groundwater levels), the uplift resistance of underground structures must be considered. The impact of groundwater buoyancy on underground structures primarily manifests in the uplift deformation and reduced stiffness of the structure. When the buoyancy force exceeds the weight of the underground structure, it results in upward uplift deformation. Meanwhile, the deformation of the surrounding retaining walls and other supporting structures is constrained by the soil, leading to the inconsistent vertical deformation of different parts of the underground structure and potentially causing cracking and damage to the structural components. Additionally, under significant uplift forces,

stiffness reduction becomes more severe after structural damage [5]. However, current industry standards lack explicit provisions for the uplift-resistant design of underground structures. As a result, devising effective uplift-resistant measures has become a primary focus for researchers [6].

In civil engineering, uplift-resistant measures typically involve the use of anchor rods [7] and uplift piles. However, the resistance provided by anchor rods is often limited and cannot adapt to the increasing depth of underground structures. As a result, large-scale uplift piles have become an effective solution to this problem. Traditional reinforced concrete uplift piles exhibit apparent flaws, such as the deformation and cracking of the concrete shell under the influence of groundwater buoyancy, potentially exposing the internal reinforcing steel. Moreover, high-concentration ions in groundwater (e.g., chloride and sulfate ions) can come into contact with the steel, leading to corrosion and the possible failure of the uplift piles [8,9]. Ongoing research aims to improve the durability and safety of uplift piles in corrosive environments while minimizing their usage costs.

To date, a significant amount of research on conventional uplift piles has been carried out. In recent years, new technologies have emerged, such as prestressed [10], branched, expanded-base piles [11], and post-grouting methods [12]. These advancements have garnered widespread attention and have led to the development of various mechanical models, enhancing our understanding of the mechanical mechanisms of uplift piles. For instance, Chattopadhyay and Pise [13] took into account the aspect ratio of the pile, surface roughness, and soil properties when studying the ultimate uplift bearing capacity of piles in sandy soil. They also proposed a method for estimating the ultimate bearing capacity of uplift piles. Shelke and Patra [14] observed that during the pile uplift process, soil displacement causes a deflection in the direction of the normal stress on the pile's side. Based on this observation, they introduced a calculation method for the fractional resistance of piles in the lateral direction. Zhu and Yang [15] investigated the influence of the Winkler model's spring stiffness, unified ultimate friction parameters, and overlying soil layers on the ultimate bearing capacity of uplift piles using theoretical derivation and program compilation. Beyond the advancements in mechanical mechanism analysis and numerical simulation methods, researchers have also conducted targeted model tests and in situ tests on uplift piles. For example, Qian et al. [16] performed a centrifuge model test on side-grouted uplift piles. They examined the effects of grouting on contact surface properties, load–displacement curves of uplift piles, and pile-side friction resistance, and compared the centrifuge model test results with in situ test outcomes. Faizi et al. [17] conducted small-scale physical tests on three groups of short piles with slenderness ratios of 2, 3, and 4, studying the uplift performance of short piles in loose sand. They also employed particle image velocimetry and close-range photogrammetry techniques to observe the deformation patterns of short piles. Similarly, Zhu et al. [18] carried out static load tests and pile body axial force tests on ultra-long bored cast-in-place piles in soft soil foundations, exploring the bearing capacity characteristics and load transfer mechanisms of these piles in soft soil foundations.

Moreover, Wang et al. [19] tested rock-socketed waveform piles for uplift resistance, finding that the hyperbolic model better fits the load–displacement curve. Feng et al. [20] conducted field tests to study the bearing capacity and failure mechanism of micro screw anchor piles, providing a valuable reference for further research and analyses. Ni et al. [21] employed the bond-slip model at the fiber-reinforced polymer–concrete interface and nonlinear spring elements to describe the bond-slip behavior between interfaces in piles and developed a finite element model to investigate the factors influencing the uplift performance of piles. Emirler et al. [22] conducted a study using Plaxis 3D to investigate the performance of single uplift piles in sand. They found that the uplift capacity positively correlates with the sand's embedment ratio and relative density, and that steel piles have a higher bearing capacity than aluminum and Delrin piles. Wang et al. [23] conducted model tests on rock-socketed piles under axial and oblique loads, revealing a lower uplift capacity and sudden failure under oblique loads. Han et al. [24] analyzed embedded and

non-embedded retaining pile walls using finite element methods, performing a parametric analysis for both types. In conclusion, current research on uplift piles primarily concentrates on developing innovative pile types and uncovering their failure characteristics, bearing mechanisms, lateral friction resistance, and ultimate bearing capacity [25–27]. Despite these advancements, conventional reinforced concrete uplift piles continue to be the primary choice in engineering practice, making it challenging to avoid the inherent limitations of traditional pile types. As a result, the research and promotion of new pile types are crucial.

In this study, a novel composite-anchor-rod uplift pile is designed to overcome the limitations of traditional uplift piles. This innovative design incorporates steel strands, non-expansive high-strength grout, and high-strength steel pipes as the main reinforcement. It aims to tackle several core issues associated with conventional uplift piles, such as overly high reinforcement ratios, material waste, poor stress performance, a tendency to crack, and insufficient durability. Firstly, the article provides a detailed description of the new pile's basic structure, along with its construction and inspection procedures. Following this, three sets of full-scale in situ static load tests are conducted to thoroughly analyze the fundamental mechanical properties and load transfer mechanisms of the new composite-anchor-rod uplift piles, comparing them to conventional reinforced concrete piles. Furthermore, a practical numerical simulation method is established for this new pile type, enabling the simulation and analysis of its bearing characteristics under uplift loads. The findings indicate that, at an extremely low reinforcement ratio of just 0.75%, the new pile type achieves equal or superior uplift resistance compared to conventional concrete uplift piles, which have a reinforcement ratio of 3.84% [28]. When designing the structure of the new composite-anchor-rod uplift piles, the cracking factor can be disregarded, leading to a reduction in reinforcement usage, lower costs per pile, and shorter construction durations. The steel reinforcement content for conventional anti-floatation piles is approximately 200 kg/m^3. However, by using a new type of composite-anchor pile, the steel reinforcement content can be reduced to 70 kg/m^3. This article also compares and summarizes the design and construction of several projects. In comparison to traditional piles, the new uplift pile design reduces the reinforcement ratio by 80%, and the cost by over 30%.

2. Design and Construction Technology of Piles

In this study, an experimental site was carefully chosen after thorough selection and comparison for pile construction and in situ loading tests. The site comprises a simple and uniform stratum consisting of a sandy soil layer and a silty soil layer, which effectively eliminates the influence of soil layer variability on the experimental results of the piles [29]. The detailed soil stratigraphic distribution is shown in Figure 1. The ground elevation of this test site is 23.49 m, the pile driving elevation is 21.00 m, and the elevation of the top of the test pile is 19.50 m.

Three types of test piles, namely KB1, KB5, and KB6, were constructed at the experimental site. Details of each type of pile foundation can be found in Table 1. KB1 is the conventional reinforced concrete uplift pile, while KB5 and KB6 are the newly developed composite-anchor uplift piles. The construction material of the pile body is C35 concrete. It should be pointed out that in order to compare the differences between them, the three types of piles use two different hole-forming methods.

Table 1. Description of the tested piles in this study [30].

Pile ID	Diameter (mm)	Length (m)	Hole-Forming Method	Estimated Uplift Bearing Capacity (kN)	Maximum Applied Load (kN)
KB1	800	22	Mud rotary drilling	4400	6600
KB5	800	22	Mud rotary drilling	4400	5280
KB6	800	22	Dry rotary drilling	4800	6240

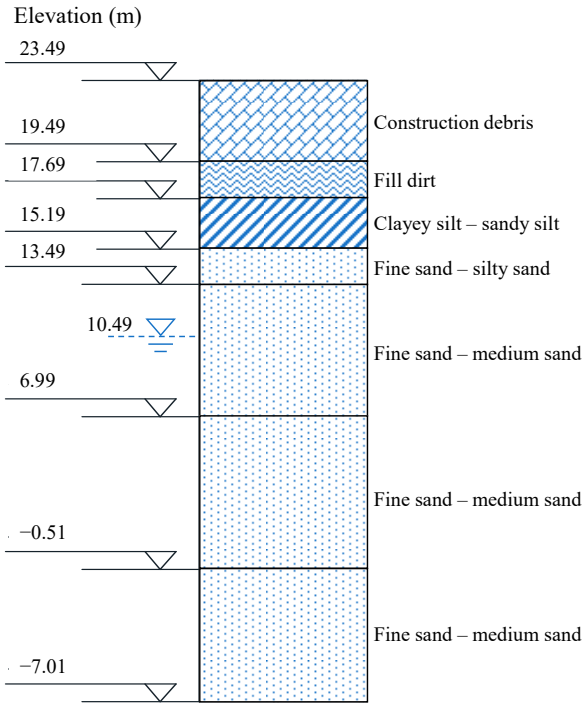


Figure 1. Schematic diagram of the soil stratigraphic distribution.

2.1. Conventional Reinforced Concrete Pile

Figure 2 illustrates the fundamental structures of the test piles. As depicted in Figure 2a, the conventional pile, denoted as KB1, employs 24 HRB400-type steel bars as its primary reinforcement. These main bars are uniformly distributed along the circumference and securely joined with spiral stirrups and stiffener rings through spot welding. The pile cage measures 23.5 m in length and has a diameter of 660 mm. To ensure precise control over the outer concrete layer thickness, which is set at 70 mm along the pile body, a total of 12 concrete spacers are arranged into three groups on the cage. Additionally, two opposing tubes for acoustic measurements are welded onto the inner side (i.e., the stiffener ring) of the pile cage.

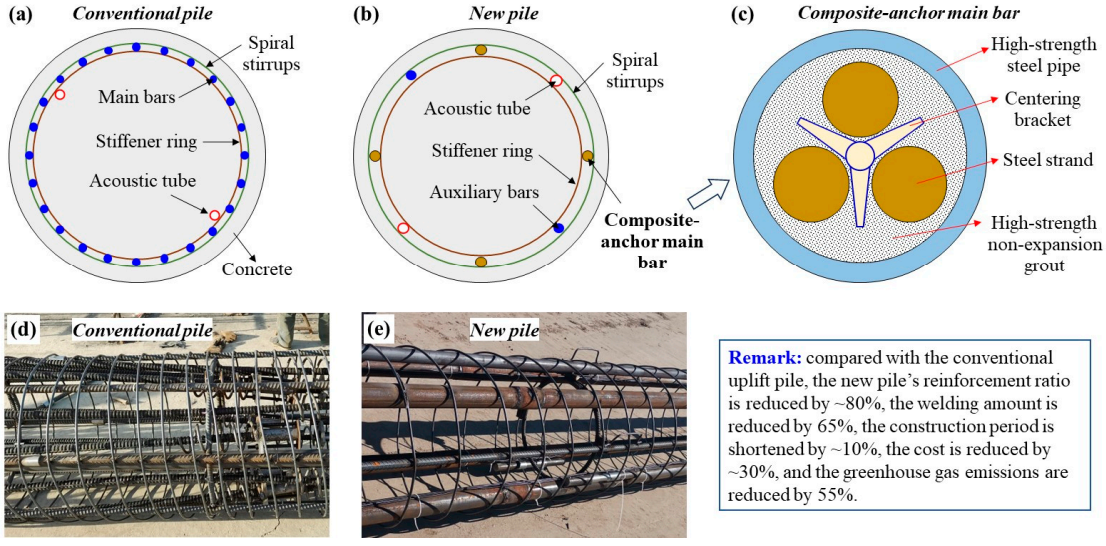


Figure 2. Structure diagram of piles and the composite-anchor main bar: (**a**) conventional reinforced concrete uplift pile; (**b**) new uplift pile with composite anchor; (**c**) composite-anchor main bar; (**d**) and (**e**) typical photos of pile cages for the conventional pile and the new pile, respectively.

The rotary drilling method was employed to create the hole for the conventional reinforced concrete pile. The permissible tolerances for pile position and diameter are 50 mm, while the acceptable verticality deviation is set at 0.8%. Furthermore, strict control is exercised to ensure that the thickness of debris accumulated at the bottom of the hole does not exceed 150 mm. It is imperative that the hole-forming process is executed continuously in a single operation. Once the hole is completed, the pile cage is lifted and inserted into the hole for subsequent concrete pouring. The time gap between the hole's completion and the initiation of concrete pouring should not exceed 4 h. The allowable tolerance for the cage installation depth is $\pm$100 mm, and the filling factor is required to exceed 1.10.

2.2. Newly Developed Composite-Anchor Pile

Figure 2b depicts the fundamental structure of the new composite-anchor uplift pile, which comprises key components such as the composite-anchor main bar, the stiffener ring, the auxiliary bar, and the spiral stirrups. In contrast to the conventional one, the main bar in this new pile consists of a composite-anchor cable comprising three steel strands (Φ_s = 21.8 mm), a high-strength steel pipe (inner diameter 65 mm, wall thickness 3.5 mm), and a specific quantity of high-strength non-expansion grout, as illustrated in Figure 2c. A total of four composite-anchor main bars were utilized within the pile structure. Additionally, to ensure the pile cage maintains a relatively circular shape, a pair of auxiliary bars and acoustic measuring tubes were evenly distributed along the same radius. Typical photographs of the pile cages are presented in Figure 2e.

It should be noted that the bottom ends of the high-strength steel pipes were closed by welding, and a water pressure test was performed on each steel pipe to ensure a good seal. The construction of the pile cage involved spot welding together the high-strength steel tubes, acoustic tubes, auxiliary bars, stiffener rings, and spiral stirrups. Once the pile cage was assembled, the top end of the steel pipe was sealed with a plug and wrapped with tape to prevent concrete from entering the steel pipe during piling. Then, a drilling machine was used to create holes, and upon hole completion, the pile cage was lifted and inserted into the hole for subsequent concrete pouring.

After the pile body was formed, high-strength non-expansion grout was carefully injected into the steel pipe to fill the cavity effectively. Subsequently, a bundle consisting of three steel strands was expertly bound together and inserted into the steel pipe, contributing to the overall reinforcement of the pile structure. To ensure a good filling of the space in the steel pipe, extra grout was added to the steel pipe. The new composite-anchor uplift pile is suitable for different construction methods, such as dry rotary drilling and mud rotary drilling. After the completion of the pile constructions, the integrity of the pile body was tested using a low-strain dynamic method and an ultrasonic method. It should be noted that in this paper, the steel strands were not prestressed. For the prestressed semi-bonded composite-anchor piles, a detailed discussion is presented in another paper.

2.3. Monitoring of Internal Stress

To assess the internal stress of the piles, rebar stress meters were utilized. Six specific sections along the pile body were carefully chosen for the installation of these meters. The layout of the rebar stress meters within the pile cages is illustrated in Figure 3a,b. The rebar stress meters can measure a maximum tensile stress of 200 MPa, exhibiting a resolution better than 0.05% FS. Moreover, they operate efficiently within a broad temperature range of $-$10 to 50 °C and demonstrate resilience to water pressure, withstanding up to 1 MPa. More detailed information about pile stress monitoring can be found in Mao et al. [29], which will not be repeated here.

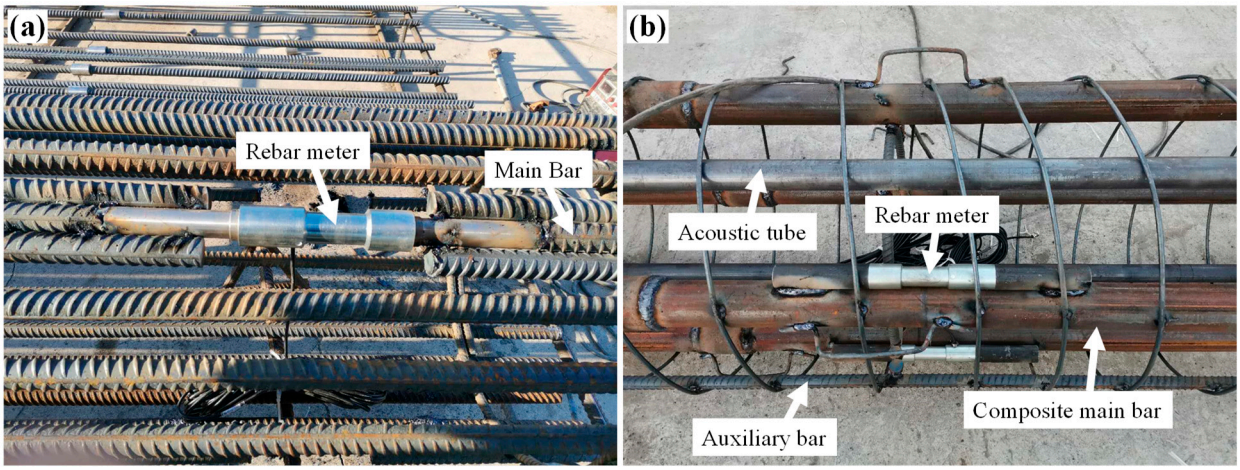


Figure 3. Typical photos of the pile cages: (**a**) the conventional pile; (**b**) the new pile.

3. Field Testing on the Pile's Bearing Characteristics

After the construction of test piles was completed, static load tests were conducted to test the bearing characteristics of the piles. The tests were carried out in accordance with the "Technical Code for Testing of Building Pile Foundations" (JGJ106-2014) [31] and the "Technical Code for Building Pile Foundations" (JGJ94-2008) [28]. It should be noted that, for the conventional piles, the load is applied to the main bars, while for the new piles, the load is applied to the steel strands.

During the field test, it is noteworthy that the Linear Variable Differential Transformer (LVDT) was employed to measure the displacement of the pile top. The LVDT used in the study has a maximum measurement range of 50 mm, with a measurement error of less than 0.25% FS and an operating temperature range of −35 to 80 °C. Detailed information about the test procedures can also be found in Mao et al. [29].

3.1. Experimental Curves of U versus δ

The experimental findings for various piles are depicted in Figures 4 and 5. Figure 4 showcases the *U*–*δ* curves, representing the relationship between the uplift load (*U*) and the displacement of the pile top (*δ*). On the other hand, Figure 5 exhibits the time courses of *δ* in a semi-logarithmic coordinate. In the case of the KB1 pile, the *U*–*δ* curve demonstrates a gradual increase in uplift displacement during the initial loading stage. However, once the load surpasses a certain threshold, the displacement suddenly experiences a steep rise, indicating a significant change. In contrast, the uplift displacement for the KB5 and KB6 piles exhibits a gradual rise with increasing load, indicating a more gradual change in behavior. According to the test results, the uplift bearing capacity and corresponding uplift displacement of each pile can be obtained, as shown in Table 2.

Table 2. Uplift bearing capacities of the three test piles.

Pile ID	Uplift Bearing Capacity (kN)	Maximum Uplift Displacement (mm)
KB1	6160	21.40
KB5	5280	23.73
KB6	6240	35.82

Moreover, a close examination of the *U*–*δ* curves reveals that the initial loading section shows similar uplift displacements among the different piles. However, as the load continues to increase, the displacement of the new piles (KB5 and KB6) gradually surpasses that of the conventional pile (KB1). A comparison between the KB1 and KB5 piles indicates that the uplift bearing capacity of the KB1 pile is approximately 16.7% higher than that

of the KB5 pile. Additionally, the maximum uplift displacement of the KB1 pile is about 9.8% lower than that of the KB5 pile, implying that the KB1 pile exhibits a more effective resistance to uplift forces compared to the KB5 pile. Importantly, both the KB1 and KB5 piles exceed the estimated bearing capacity of 4400 kN, satisfying the design requirements for uplift bearing capacity. In contrast, a comparison between the KB5 and KB6 piles reveals that the bearing capacity of the KB6 pile is approximately 18.2% higher than that of the KB5 pile. This significant difference can be attributed to the implementation of the dry rotary drilling method for hole formation in the KB6 pile, which eliminates the mud skin effect between the pile body and the surrounding soil. Furthermore, when compared to the KB1 pile, the uplift bearing capacity of the KB6 pile shows an increase of approximately 1.3%.

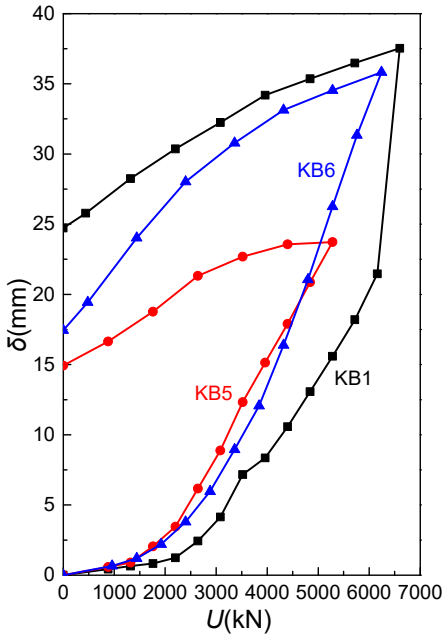
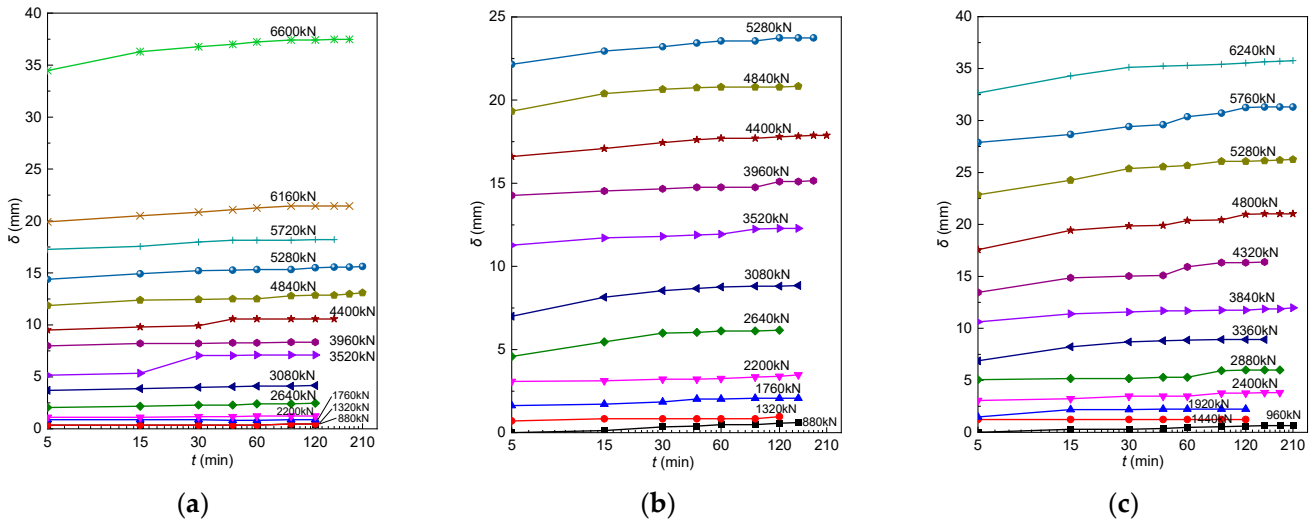


Figure 4. Experimental U–δ curves for test piles.



(**a**) (**b**) (**c**)

Figure 5. Time courses of δ for different test piles: (**a**) KB1; (**b**) KB5; (**c**) KB6.

3.2. Analyses of Axial Force

The distribution of axial force along the piles is depicted in Figure 6. It is evident that the axial force in the pile body gradually decreases downward. Examining the experimental curves, the KB1 pile exhibits a rapid decrease in axial force within the elevation range

of −1 m to −7.5 m, while the decrease in axial force becomes relatively slight within the elevation range of −18 m to −21.5 m. Intuitively, the elevation of −7.5 m can be considered as the turning point for the gradient of axial force. In the case of the KB5 pile, the axial force changes in a stepped manner, with a slow decrease within the elevation range of −1 m to −4 m, a faster decrease within the elevation range of −4 m to −7.5 m and −7.5 m to −14 m, and a slow decrease again within the elevation range of −18 m to −21.5 m. Table 3 presents a comprehensive overview of the pile's lateral friction resistance distribution. By comparing the results between KB1 and KB5, notable differences can be observed. The KB1 pile primarily experiences significant stress in the upper region of the pile body, indicating that the full potential of lateral friction resistance in the lower portion of the pile is not fully utilized. In contrast, the forces acting on the KB5 pile are predominantly concentrated in the middle section of the pile body, suggesting a more balanced and efficient distribution of lateral friction resistance along its entire length.

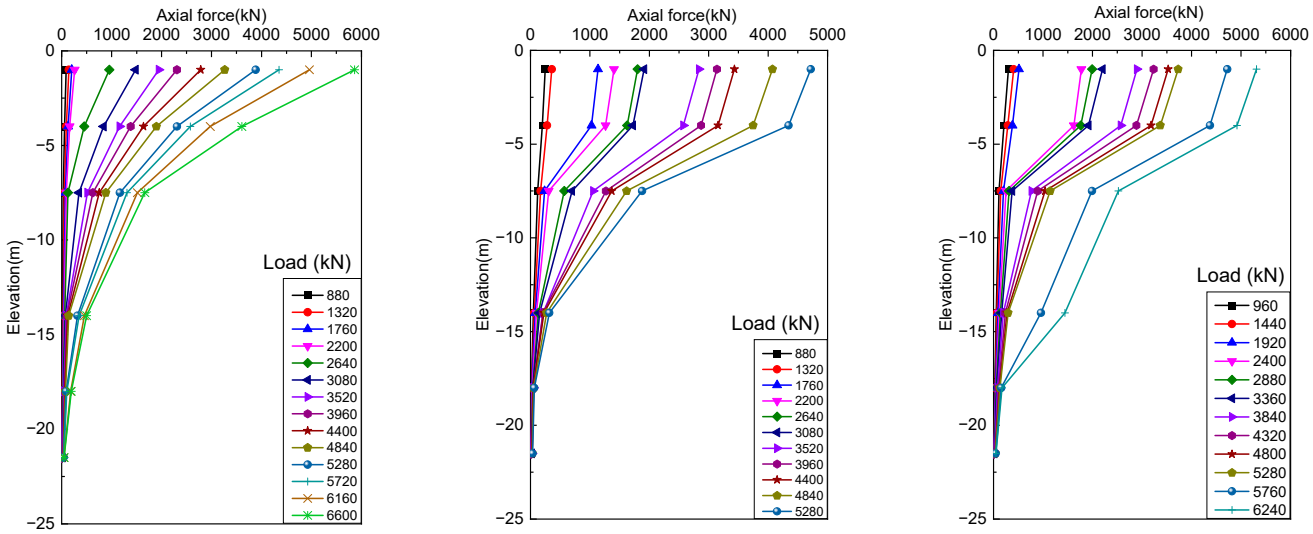


Figure 6. Distribution of axial force in piles under different loads: (**a**) KB1; (**b**) KB5; (**c**) KB6.

Table 3. Experimental results of developed resistance of lateral friction under a load of 5280 kN.

Elevation (m)	Lateral Friction Resistance (kPa)		
	KB1	KB5	KB6
−1~−4	209.3	51	47.8
−4~−7.5	129.8	268.4	273.1
−7.5~−14	52.1	90.7	51.9
−14~−18	22.4	23.9	26.6
−18~−21.5	3.1	3	10.6

The axial force distribution characteristics in both the KB5 and KB6 piles exhibit a similar pattern. Notably, the axial force in both piles undergoes significant attenuation within the elevation range of −4 m to −7.5 m. Within this range, the lateral friction resistance of the KB6 pile slightly surpasses that of the KB5 pile. Furthermore, at the elevation range of −18 m to −21.5 m, the lateral friction resistance of the KB6 pile is 3.5 times greater than that of the KB5 pile. This signifies that the KB6 pile demonstrates superior uplift bearing capacity characteristics, as it enables a better utilization of lateral friction resistance in the lower portion of the pile under uplift loads when compared to the KB5 pile.

The distribution of lateral friction resistance in the KB1 pile primarily occurs within the elevation range of −1 m to −7.5 m, while in the KB6 pile, it predominantly takes place

within the range of −4 m to −7.5 m. Notably, the maximum lateral friction resistance of the KB6 pile is approximately 30% higher than that of the conventional KB1 pile. Specifically, in the elevation range of −18 m to −21.5 m, the lateral friction resistance of the KB6 pile is 3.5 times greater than that of the KB1 pile. These findings indicate that the KB6 pile effectively utilizes the lateral friction resistance in the middle and lower regions of the pile body, resulting in an improved stress state compared to the KB1 pile.

According to the data presented in Table 3, the conventional pile (KB1) primarily experiences stress in the upper section of its pile body, whereas the new piles (KB5 and KB6) mainly bear stress in the lower section. To illustrate the force transmission mechanism of these two types of piles under uplift loads, Figure 7 provides a schematic diagram. In conventional uplift piles, when the ribbed steel main bar is subjected to pulling forces, the load will be quickly transferred to the adjacent concrete. As such, the influence of the uplift load is mainly concentrated on the upper pile body, where the axial force of the pile body changes drastically. However, in the range of the middle and lower part of the pile, the load transmitted by the main bars becomes smaller, with minor changes in the axial forces. On the other hand, in the new composite-anchor piles, when the composite-anchor main bar is subjected to pulling forces, the load will be gradually transferred to the pile concrete through the three interfaces of steel wire: rope–grouting body, grouting body–high-strength steel pipe, and steel pipe–pile concrete. The transfer of load between the interfaces in the new piles results in a more uniform distribution of load, and the action range of the load extends to the middle section of the pile. As a result, the distribution of axial force in the new piles is smoother compared to the conventional uplift pile. This indicates that the new pile design improves the load transmission characteristics and leads to a more balanced distribution of the axial forces along the pile body.

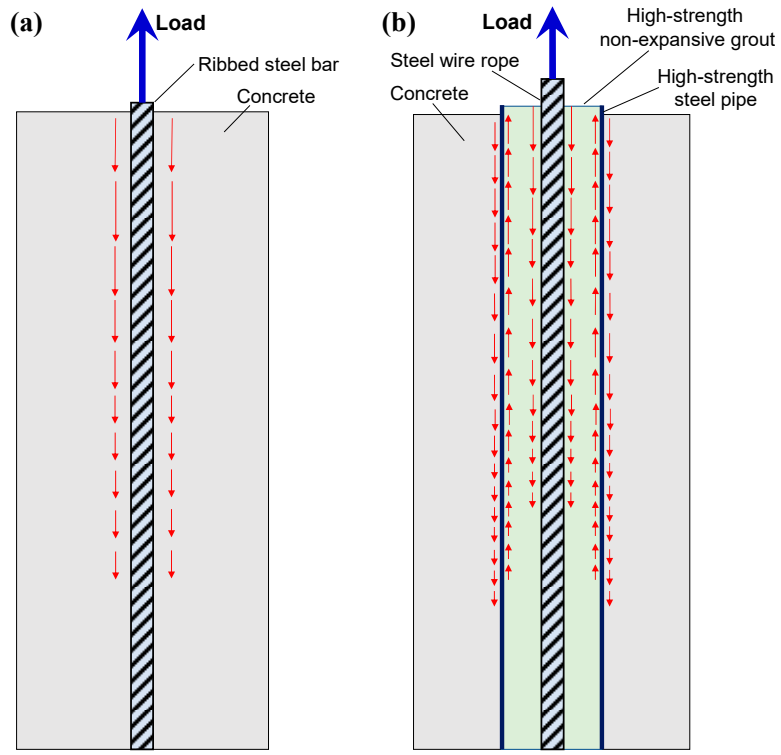
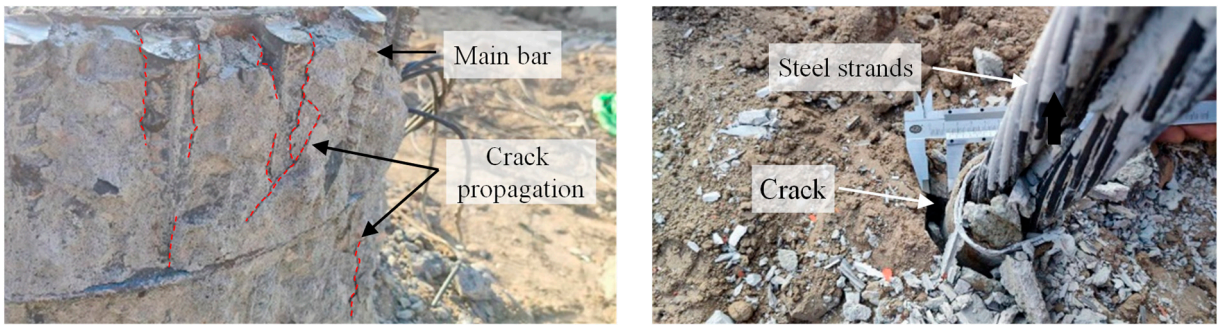


Figure 7. Schematic diagram of force transmission mechanisms of the types of uplift piles: (**a**) the conventional uplift piles; (**b**) the new type of composite-anchor uplift pile.

3.3. Analyses of Pile Cracks

Figure 8 shows typical photos of cracks that occurred on the top of the two kinds of uplift piles after static load tests. Results show that the cracks in the two piles are close to

the main bars. For the conventional uplift pile (i.e., KB1) with a relatively higher ratio of reinforcement (i.e., 3.84%), the axial force at the top part of the pile decays sharply, and the cracks on the pile top appear small and dense (Figure 8a). These cracks provide a channel for groundwater to contact the main reinforcement, which is not conducive to the serviceability of the pile.



(**a**) (**b**)

Figure 8. Typical photos of cracks that occurred at pile heads: (**a**) the conventional uplift pile; (**b**) the new composite-anchor uplift pile.

For the new type of uplift piles (i.e., KB5 and KB6), the main reinforcement of the pile body is composed of only four composite-anchor cables, which have a much lower ratio of reinforcement (i.e., 0.75%). As shown in Figure 8b, the cracks on the top pile are concentrated near the composite main bars, and they are relatively wide but sparse. There are no lateral cracks in the pile, so it is difficult for groundwater to contact and erode the main reinforcement along the lateral direction. In addition, the new piles adopt the composite anchor as the main bars, and the load-bearing steel strands were further protected by the grouting body and the high-strength pipe, which provide a stronger resistance to groundwater erosion.

From the previous analyses, it can be observed that conventional reinforced concrete piles exhibit a higher occurrence of cracks at the top of the pile, whereas the new composite-anchor piles demonstrate fewer cracks. This can be attributed to the distribution characteristics of forces along the piles. The conventional uplift piles experience significant stress concentration in the upper part, resulting in a sharp variation in axial force and considerable strain at the top of the pile. Consequently, cracks tend to develop in this region. On the other hand, the new uplift piles primarily bear stress in the middle and lower sections, leading to reduced cracking at the pile top. The more uniform distribution of forces in the new piles contributes to the mitigation of crack formation in this area.

4. Numerical Analysis of Uplift Capacity in Composite-Anchor Piles

Drawing on previous discussions about pile materials, foundation characteristics, and in situ test results, this study seeks to develop a numerical model that accurately captures the stress-deformation features of composite-anchor-rod uplift piles. The goal is to offer theoretical foundations and technical support for the structural optimization, design, and engineering applications of these new uplift piles.

Under uplift loads, the displacement of the pile body primarily results from the elastic deformation of pile materials and slippage at the interface. It is also influenced by the foundation's mechanical properties. Considering these factors, the numerical model simplifies each material within the pile body as a linear elastic material, while each soil layer in the pile-side foundation is defined as a Mohr–Coulomb cohesion–friction material. As the composite-anchor-rod uplift pile undergoes the uplifting process within the foundation, the mechanical properties of the interfaces between different materials significantly impact the pile's load-bearing characteristics. Consequently, the numerical model establishes four contact surfaces at the interfaces of the foundation: soil–pile body, concrete pile

body–high-strength steel pipe, high-strength steel pipe–grout, and grout–steel strand. The tangential behavior of these four contact surfaces is represented using the Coulomb friction model [32], and the normal direction is defined as hard contact. Taking into account the initial stress field generated by the soil's self-weight, vertical loads are applied through displacement control.

The dimensions, structure, and foundation soil layer distribution of the uplift pile in the numerical model are determined based on field tests. The new composite-anchor pile has a diameter of 800 mm and a height of 22 mm, while the diameter of the pile-side soil is 16 m, and the total depth of the soil body is 30 m. As depicted in Figure 9, a detailed model of the composite-anchor pile structure is created, encompassing 146,987 elements and 161,456 nodes. The uplift pile itself contains 112,037 elements and 124,612 nodes. The element and node numbers of the composite-anchor pile constitute 76.2% and 77.2% of the entire model, respectively. The parameters for each pile material in the model can be found in Table 4. The properties of the pile-side soil are sourced from the test site's "Geotechnical Engineering Investigation Report". The foundation soil is mainly composed of silt and sand and can be further divided into six layers. The parameter values for each soil layer are provided in Table 5.

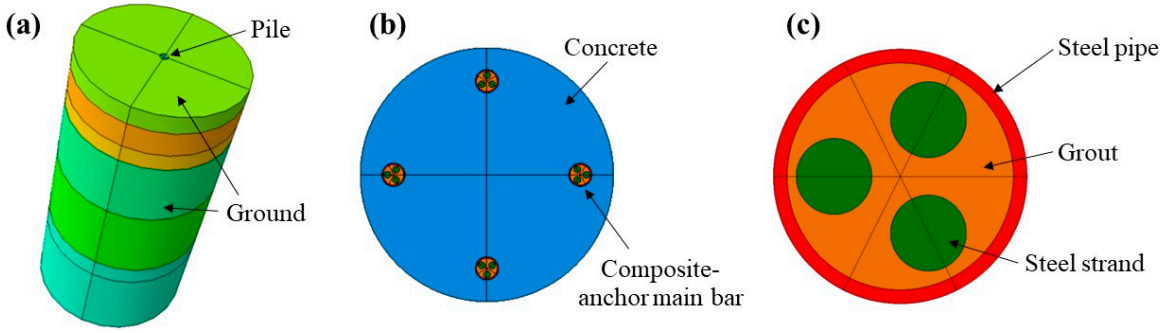


Figure 9. Three-dimensional pile–soil interaction model used in the numerical simulation: (**a**) overall model setup; (**b**) cross-section of the new composite-anchor pile; (**c**) enlarged detail of the composite anchor.

Table 4. Basic material properties of composite-anchor pile.

Material	Density ρ (kg/m^3)	Elastic Modulus E (MPa)	Poisson's Ratio ν
Steel strand	7.85×10^3	1.95×10^5	0.28
Rout	1.80×10^3	2.50×10^4	0.20
High-strength steel pipe	7.85×10^3	2.10×10^5	0.30
C35 concrete	2.30×10^3	3.15×10^4	0.18

Table 5. Physical properties of ground soil from top to bottom.

Soil Layer	Thickness h (m)	Density ρ (kg/m^3)	Cohesion c (MPa)	Friction Angle ϕ (°)	Elastic Modulus E (MPa)	Poisson's Ratio ν	Pile-Side Ultimate Friction q (MPa)
1	1.8	1.9×10^3	0.01	10	6.2	0.33	0.03
2	2.5	1.94×10^3	0	24	7.6	0.33	0.045
3	1.7	1.95×10^3	0	25	20	0.33	0.04
4	6.5	2.0×10^3	0	28	30	0.33	0.06
5	7.5	2.05×10^3	0	30	45	0.33	0.065
6	10.0	2.05×10^3	0	30	55	0.33	0.070

Employing the aforementioned model and parameters, finite element calculations were conducted on the new anchor-cable pile. Figure 10 displays a comparison between

the calculated load–displacement (U–δ) curves of the new anchor-cable pile and the field test measurements. As seen in the figure, under various uplift loads, the finite element simulation results for the pile-top displacement closely correspond with the measured results. The maximum difference is approximately 0.5 mm (under a load of 5280 kN), and the error rate is about 2.2%. Additionally, both the simulated and measured U–δ curves show a gradual change. In general, it can be concluded that the established numerical model is reasonably reliable and can be used to simulate the uplift process of composite-anchor uplift piles.

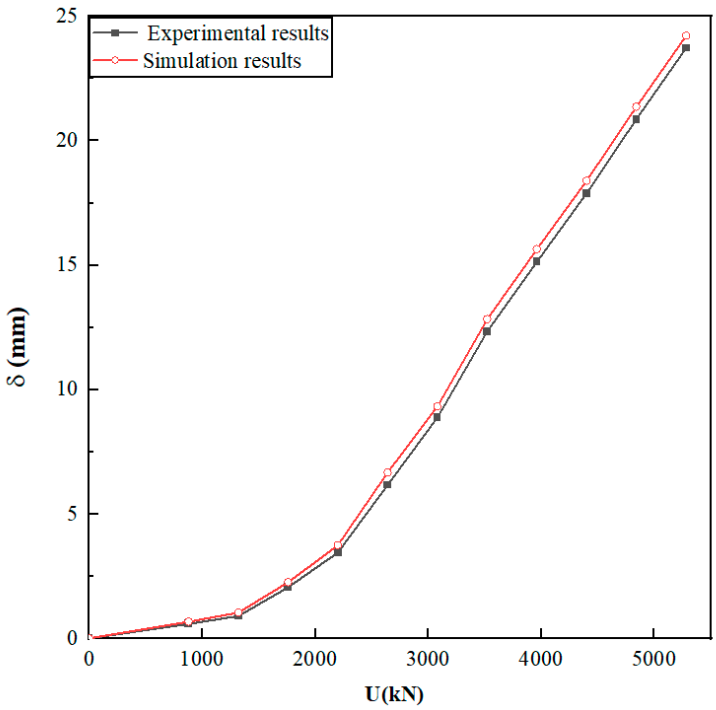


Figure 10. Comparison of calculated and experimental results of the new pile's U–δ curve.

As demonstrated in Figure 11b,c, the stresses in the steel pipe and steel strand progressively increase with the load level and decrease incrementally along the z-direction with depth. However, once the load level reaches seven, the stress at the top of the steel pipe and steel strand in the z-direction remains constant, while the stress in the lower part continues to rise incrementally. Furthermore, when the axial tension is low, the load of the steel strand is uniformly transmitted to the steel pipe through the contact surface of the composite anchor, resulting in an even stress distribution at the top of the composite anchor. As the load escalates to a certain degree, the stress at the top of the composite anchor reaches its limit and is transferred to the lower part via the contact surface. Consequently, the stress in the middle and lower parts of the composite anchor increases rapidly, and the composite anchor as a whole experiences a uniform stress distribution.

Figure 11 illustrates the distribution of calculated stress in the z-direction for the concrete, high-strength steel pipe, and steel strand within the composite-anchor uplift pile under various load levels. As depicted in Figure 11a, the stress in the pile body is tensile, decreasing with depth while increasing with the load level. The stress in the concrete at the top of the pile remains relatively constant, declines at the bottom, and intensifies while concentrating on the pile body. This suggests that as the load increases, the contact surface at the top of the composite anchor reaches its limit bond strength and starts to slip, causing the main stress point to shift downward and leading to an alteration in the overall stress distribution of the pile body.

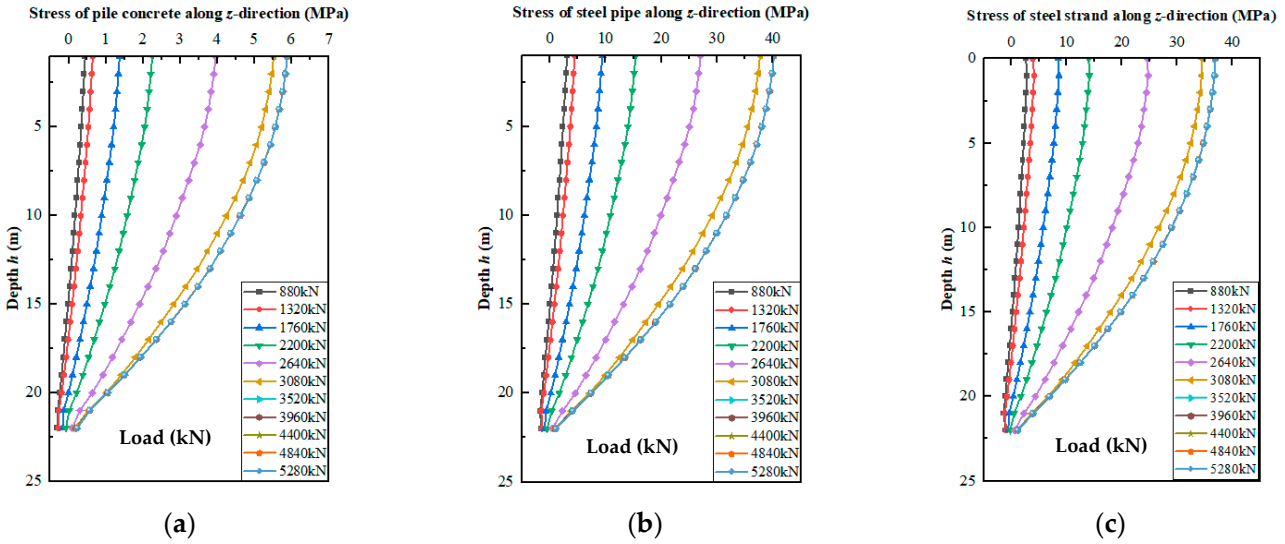


Figure 11. *z*-direction stress curves of different components under various load levels: (**a**) stress of the pile concrete along the *z*-direction; (**b**) stress of the steel pipe along the *z*-direction; (**c**) stress of the steel strand along the *z*-direction.

5. Discussion

This study proposes a new composite-anchor pile as an alternative to conventional uplift piles, addressing key concerns related to crack resistance and corrosion resistance. One of the significant advantages of this innovative solution is its remarkably lower reinforcement ratio, which stands at just 0.75% compared to the relatively high 3.84% reinforcement ratio of conventional uplift piles. This reduction in the reinforcement ratio results in substantial cost savings during the manufacturing of the reinforcement cage and overall pile construction. Moreover, the construction of composite uplift piles is notably faster when compared to conventional piles. The successful application and verification of this new pile type in various engineering projects, including the Anti-floating Project of Hyatt Place Hotel in Huangshan, Hengjiang Bay and the Beijing Tongzhou Comprehensive Transportation Hub Project, further bolster its credibility. Upon conducting a thorough comparison between the design and construction of several actual projects, the new composite-anchor pile demonstrated remarkable cost effectiveness. Compared to conventional uplift piles, there is a 65% reduction in the required welding amount, a reduced construction period by approximately 20%, a reduction of approximately 30% in construction costs, and a decrease in greenhouse gas emissions by 55%. These advantages make the new composite-anchor pile an attractive and promising choice for foundation engineering projects. However, it is important to consider certain factors in the engineering application of the new composite-anchor pile. Several issues warrant attention regarding its uplift performance. The following discussion will elaborate on these considerations for a better understanding and implementation of the new pile design in practical projects.

First of all, the uplift displacements of the new piles are greater than that of the conventional piles, which may be related to the different crack properties of the pile body during the static load tests. When cracks occur in the pile, the originally tensioned concrete retracts to both sides of the crack like a broken rubber band, but this retraction is not free and is constrained by the main bars. The KB1 pile adopts 24 ribbed steel bars as the main reinforcement; a higher ratio of reinforcement makes the resistance to concrete cracking and shrinking greater, so that the cracks are relatively fine and densely distributed. The KB5 and KB6 piles adopt four composite-anchor cables as their main reinforcement, which have a much lower reinforcement ratio. Moreover, the outer surface of the composite anchor is relatively smooth. When the concrete is cracked, the restraining force of the main reinforcement is smaller, resulting in greater uplift displacements. In response to this issue, corrugated pipes can be used in future engineering applications to replace the current

high-strength steel pipes. On the other hand, the contact area between the composite anchor and the pile concrete can be appropriately increased by using thicker steel pipes.

In addition, a lower reinforcement ratio of the new pile makes the stress more likely to concentrate near the interface between the main bars and the pile body. The uneven distribution of stress in the cross-section of the pile will further cause shear failure in the upper pile, resulting in longitudinal cracks and a corresponding increase in the pile's uplift displacement. To solve this issue, the number of composite main bars can be increased to improve the uniformity of stress distribution while maintaining economic efficiency. For example, the scheme of six composite-anchor main bars with two steel strands in each can be used to make the reinforcement more evenly distributed in the section of pile.

The cementing material in the composite main bar of the new pile is a high-strength non-expansion grouting body, which keeps a constant volume during the curing process, ensuring that the grouting body is filled tightly between the high-strength steel pipe and the steel strands after solidification. In fact, other kinds of grouts that can meet the above requirement could also be used to replace the currently used product, so as to achieve the purposes of lower cost and better durability. The corrosion resistance of the main bars can be further improved by replacing the currently used steel piles with other corrosion-resistant pipes, such as the high-strength plastic piles and high-strength polymer-casing pipes.

In situ experimental results show that the new uplift pile with the hole-forming method of dry rotary drilling can improve the pile's lateral friction resistance and the uniformity of axial force, which enhances the ultimate bearing capacity of the pile. According to the stress characteristics, the new pile can be further constructed in combination with prestressing, post-grouting, and bottom expansion to improve the utilization of the pile's lateral friction resistance and increase the pile's ultimate bearing capacity, with little changes to the cost and construction period.

Another concern is that the frictional resistance of a pile is mainly affected by the interaction between the pile surface and the surrounding soil. Although stratigraphy has some influence on frictional resistance, this is not the focus of this study. The stratigraphy or soil conditions encountered in the construction process will indeed affect the performance of friction to a certain extent, but in this study, these are considered to be secondary factors that can be ignored. On the one hand, the three kinds of test piles are all in the same site, and their stratum conditions are the same, so the influence of stratigraphy on the load-bearing characteristics of the test piles can be reasonably ignored in order to facilitate cross-sectional comparison. On the other hand, the site comprises a simple and uniform stratum consisting of sandy or silty soil layers, which effectively eliminates the influence of soil layer variability on the experimental results of the piles. In summary, the research focus of this paper is to design a new type of uplift pile and compare its bearing capacity and bearing mechanism with conventional ones. In other words, the type of pile is regarded as the main controlling factor affecting the bearing capacity of different pile types, while the influence of factors such as stratigraphy is not specifically discussed, and this neglect does not affect the analysis of the results.

6. Conclusions

In this study, a novel composite-anchor-rod uplift pile is designed to overcome the limitations of traditional uplift piles. Firstly, the article provides a detailed description of the new pile's basic structure, along with its construction and inspection procedures. Following this, three sets of full-scale in situ static load tests are conducted to thoroughly analyze the fundamental mechanical properties and load transfer mechanisms of the piles. Furthermore, a practical numerical simulation method is established for this new pile type, enabling the simulation and analysis of its bearing characteristics under uplift loads. The main conclusions can be drawn as follows.

(1) The new composite-anchor pile utilizes composite anchors as the primary reinforcement, which allows for the transmission of tensile forces through the interfaces between the steel strand, grouting body, high-strength steel pipe, and concrete. This

design promotes a more favorable (or a more uniform) stress distribution within the pile body. By incorporating these different components, the pile is able to achieve a better stress state, enabling it to effectively resist uplift forces and maintain its structural integrity.

(2) At a very low reinforcement ratio of just 0.75%, the new pile type achieves an equal or superior uplift resistance compared to conventional concrete uplift piles, which have a reinforcement ratio of 3.84%. When designing the structure of the new composite-anchor uplift piles, the cracking factor can be disregarded, leading to a reduction in reinforcement usage, lower costs per pile, and shorter construction durations. In comparison to traditional piles, the new uplift pile design reduces the reinforcement ratio by 80.5%, the cost by over 30%.

(3) The implementation of the dry rotary drilling method instead of mud rotary drilling has resulted in an 18.2% increase in the uplift bearing capacity of the pile. This improvement can be attributed to the avoidance of the mud skin effect between the pile body and the soil, which enhances the overall performance of the pile. By combining the composite-anchor piles with the dry holing method, not only can the uplift bearing capacity of the piles be enhanced, but there are also additional benefits such as cost reduction and shortened construction periods. The utilization of this approach offers a more efficient and cost-effective solution for uplift-resistant pile design and construction.

(4) The steel wire ropes in the new composite-anchor piles are effectively protected from the external environment, including groundwater, due to the presence of the grouting body and high-strength steel piles. This isolation provides an improved durability compared to conventional piles. By safeguarding the steel wire ropes against potential corrosion and other environmental factors, the new piles are anticipated to maintain their structural integrity and performance over an extended period. This enhanced durability is a notable advantage of the new composite-anchor piles, ensuring their long-term stability and reliability in various environmental conditions.

Author Contributions: Conceptualization, E.W.; Methodology, E.W.; Software, J.J. and H.G.; Resources, Z.M.; Data curation, J.J.; Writing—original draft, J.J. and H.G.; Writing—review & editing, E.W.; Supervision, E.W.; Funding acquisition, Z.M. All authors have read and agreed to the published version of the manuscript.

Funding: This research was funded by the Major Program of the National Natural Science Foundation of China (Grant No. 52090081) and the Joint Funds of the Department of Science and Technology of Shaanxi Province, China (Grant No. 2021JLM-54).

Data Availability Statement: The data presented in this study are available on request from the first and corresponding authors.

Conflicts of Interest: The authors declare no conflict of interest.

References

1. Broere, W. Urban underground space: Solving the problems of today's cities. *Tunn. Undergr. Space Technol.* **2016**, *55*, 245–248. [CrossRef]
2. Cheng, G.; Wang, R.; Zhao, M.; Su, J.; Yang, Y. Current situation and development trend of urban underground space development and utilization in China. *Geosci. Front.* **2019**, *26*, 39–47.
3. Hunt, D.V.L.; Makana, L.O.; Jefferson, I.; Rogers, C.D.F. Liveable cities and urban underground space. *Tunn. Undergr. Space Technol.* **2016**, *55*, 8–20. [CrossRef]
4. Zhen, Q. Development and utilization of urban underground space. *IOP Conf. Ser. Earth Environ. Sci.* **2019**, *242*, 052059. [CrossRef]
5. Jian, B.; Lu, T.; Li, S.; Yin, K. The effect of groundwater buoyancy on the structural safety of underground buildings. *Civ. Archit. Environ. Eng.* **2010**, *32*, 56–60.
6. He, L.; He, Z. Analysis of floating effect of groundwater on built underground structure. *IOP Conf. Ser. Earth Environ. Sci.* **2021**, *784*, 012030. [CrossRef]
7. Kou, H.-L.; Guo, W.; Zhang, M.-Y. Pullout performance of GFRP anti-floating anchor in weathered soil. *Tunn. Undergr. Space Technol.* **2015**, *49*, 408–416. [CrossRef]

8. Zhao, Y. Overview of rust cracking of concrete structures caused by steel corrosion. *J. Southeast Univ. Nat. Sci. Ed.* **2013**, *43*, 1122–1134.
9. Zhuang, N.; Dong, H.; Zhou, Y.; Chen, D. Cracking behavior of reinforced concrete piles externally bonded with carbon fiber reinforced polymer in a marine environment. *Constr. Build. Mater.* **2018**, *190*, 1154–1162. [CrossRef]
10. Liu, X.Y.; Zhang, X.Y.; Li, X.; Zhang, M.; Zheng, X.J. Design study of prestressed uplift cast-in-place pile. *Adv. Mater. Res.* **2011**, *308–310*, 213–216. [CrossRef]
11. Zhang, Z.H.; Yuan, M.L.; Cui, Q.; Lu, X.L.; Liu, S.Q. Definition of the ultimate state of the scooted head pile bearing uplift load in soil foundation based on failure approach index. *Adv. Mater. Res.* **2011**, *250–253*, 2481–2485. [CrossRef]
12. Liu, Y.; Hu, X.; Ma, Y.; Liu, S. Application of post-grouting technology in silty sand formation piles. *Bridge Constr.* **2019**, *49*, 127–132.
13. Chattopadhyay, B.; Pise, P. Uplift capacity of piles in sand. *J. Geotech. Eng.* **1986**, *112*, 888–904. [CrossRef]
14. Shelke, A.; Patra, N.R. Effect of arching on uplift capacity of single piles. *Geotech. Geol. Eng.* **2009**, *27*, 365–377. [CrossRef]
15. Zhu, B.; Yang, M. Deformation and ultimate bearing capacity calculation of uplift piles. *J. Build. Struct.* **2006**, *27*, 120–129.
16. Qian, J.; Ma, X.; Li, W.; Huang, M.; Wang, W. Centrifugal model test and in-situ test analysis of pile side grouting uplift pile. *Geomechanics* **2014**, *35*, 1241–1246+1254.
17. Faizi, K.; Armaghani, D.J.; Sohaei, H.; Rashid, A.S.A.; Nazir, R. Deformation model of sand around short piles under pullout test. *Measurement* **2015**, *63*, 110–119. [CrossRef]
18. Zhu, X.; Fang, P.; Huang, H. Experimental study on engineering properties of deep soft foundation ultra-long piles. *Chin. J. Geotech. Eng.* **2003**, *25*, 76–79.
19. Wang, Q.; Ma, J.; Xiao, Z.; Chen, W.; Ji, Y. Field test on uplift bearing capacity of rock-socketed belled piles. *KSCE J. Civ. Eng.* **2020**, *24*, 2353–2363. [CrossRef]
20. Feng, S.-J.; Ma, J.; Xiao, Z.; Chen, W.; Ji, Y. Field tests of micro screw anchor piles under different loading conditions at three soil sites. *Bull. Eng. Geol. Environ.* **2021**, *80*, 127–144. [CrossRef]
21. Ni, P.; Mei, G.; Zhao, Y. Numerical investigation of the uplift performance of prestressed fiber-reinforced polymer floating piles. *Mar. Georesources Geotechnol.* **2017**, *35*, 829–839. [CrossRef]
22. Emirler, B.; Tolun, M.; Yildiz, A. 3D numerical response of a single pile under uplift loading embedded in sand. *Geotech. Geol. Eng.* **2019**, *37*, 4351–4363. [CrossRef]
23. Wang, Q.; Hu, Z.; Ji, Y.; Ma, J.; Chen, W. Model test of rock-socketed pile under axial and oblique tension loading in combined composite ground. *Int. J. Geomech.* **2022**, *22*, 04022182. [CrossRef]
24. Han, J.; Wang, J.; Cheng, C.; Zhang, C.; Liang, E.; Wang, Z.; Song, J.-J.; Leem, J. Mechanical response and parametric analysis of a deep excavation structure overlying an existing subway station: A case study of the Beijing subway station expansion. *Front. Earth Sci.* **2023**, *10*, 1079837. [CrossRef]
25. He, S. Study on failure characteristics and bearing capacity of uprooted piles. *Geomechanics* **2001**, *3*, 308–310.
26. Huang, M.; Ren, Q.; Wang, W.; Chen, Z. Analysis of ultimate bearing capacity of uplift piles under deep excavation conditions. *Chin. J. Geotech. Eng.* **2007**, *29*, 1689–1695.
27. Schmertmann, J.H. Discussion of "Experimental studies on behavior of single pile under combined uplift and lateral loading" by K. Madhusudan Reddy and R. Ayothiraman. *J. Geotech. Geoenviron. Eng.* **2016**, *142*, 07016015. [CrossRef]
28. *JGJ 94-2008*; Technical Code for Building Pile Foundations. Ministry of Construction; China Architecture & Building Press: Beijing, China, 2008.
29. Mao, Z.; Guo, H.; Wu, Y.; Wang, E.; Li, X. Development of a new uplift pile with prestressed semi-bonded composite anchor. *Buildings* **2022**, *12*, 1478. [CrossRef]
30. *JGJ 476-2019*; Technical Standard for Building Engineering Against Uplift. Ministry of Housing and Urban-Rural Development; China Architecture & Building Press: Beijing, China, 2019.
31. *JGJ 106-2014*; Technical Code for Testing of Building Foundation Piles. Ministry of Housing and Urban-Rural Development; China Architecture & Building Press: Beijing, China, 2014.
32. Wang, S. Experimental and numerical analysis of the bearing performance of static driven root-planted piles. In Proceedings of the 15th National Conference on Pile Foundation Engineering, Hangzhou, China, 6–8 April 2023; p. 6.

Disclaimer/Publisher's Note: The statements, opinions and data contained in all publications are solely those of the individual author(s) and contributor(s) and not of MDPI and/or the editor(s). MDPI and/or the editor(s) disclaim responsibility for any injury to people or property resulting from any ideas, methods, instructions or products referred to in the content.